THE JOURNAL OF PHYSICAL CHEMISTRY C

Article

Cite This: J. Phys. Chem. C 2019, 123, 24731−24739

pubs.acs.org/JPCC

Plasmonic Trimers for Dual-Frequency Surface-Enhanced Two-Dimensional Infrared Spectroscopy

Robert T. Mackin,[†,⊥] Bar Cohn,[‡,⊥] Ben Engelman,[§] Adi Goldner,[∥] Igor V. Rubtsov,*[,†] and Lev Chuntonov*[,‡,§]

[†]Department of Chemistry, Tulane University, New Orleans, Louisiana 70118, United States

[‡]Schulich Faculty of Chemistry, [§]Solid State Institute, and [∥]Micro−Nano-Fabrication and Printing Unit (MNF&PU), Andrew and Erna Viterbi Faculty of Electrical Engineering, Technion—Israel Institute of Technology, Haifa 3200003, Israel

Supporting Information

ABSTRACT: Extension of surface-enhanced two-dimensional infrared spectroscopy (SE-2DIR) to dual-frequency experiments allows studying dynamics and energy transport in thin molecular films by tagging and probing vibrational modes on different sites of the molecule. Measurements of cross-peaks involving transitions largely separated in frequency by SE-2DIR require plasmonic nanostructures with resonant excitations at the corresponding frequencies, where the associated enhanced near-fields spatially overlap and different molecular transitions are simultaneously enhanced in the same molecule. Gold trimer infrared antennas localize enhanced fields within the gap formed by their arms. We exploit the symmetry of trimer antennas to individually tune frequencies of the in-plane plasmonic excitations to match molecular transitions of interest. Dual-frequency SE-2DIR measurements are demonstrated on 4-azidobutyrate-*N*-hydroxysuccinimide ester with the cross-peaks between the carbonyl and azido stretching vibrational modes, separated by 370 cm^{-1}, and the carbonyl and C−N−C stretching modes, separated by 550 cm^{-1}. Excitation with cross-polarized laser pulses allows appropriate plasmon excitations in resonance with the relevant molecular transitions to be selectively accessed. Our approach, based on the rational plasmon mode engineering, achieves significant enhancement of the cross-peak signals involving largely separated transition frequencies, which is not possible with single broadband plasmon modes.

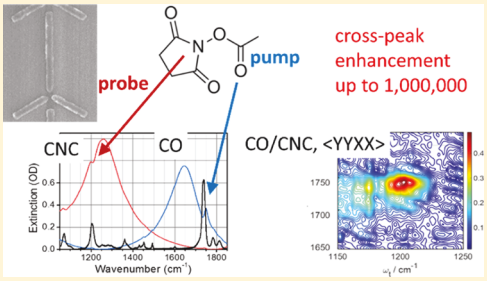

INTRODUCTION

Infrared vibrational spectroscopy is a powerful method for studies of the molecular structure for many applications, spanning from fundamental science[1] to applied medical diagnostics.[2] However, standard approaches based on measurements of linear absorption are limited in many practical aspects,[3] including dealing with peak congestion typical for samples in condensed phase, isolating useful signals from absorption backgrounds associated with the molecular environment (solvents, etc.), and measuring signals for generally weak vibrational transitions. Some of these limitations are resolved by nonlinear two-dimensional infrared spectroscopy (2DIR).[4] In 2DIR, time-dependent correlation maps between the excited and probed vibrational transitions are constructed,[5] revealing the coupling between various vibrational modes in the molecule through the corresponding cross-peaks observed in the 2D spectrum.[6] Scaling of the 2DIR peak amplitude with the square of the extinction coefficient of the vibrational transitions rather than with the square of the optical density of the absorption peaks permits greatly reducing and even eliminating contributions from weakly absorbing but abundant transitions originating from the solvent. Gaining access to information on intra- and intermolecular coupling and how it changes on the ultrafast time scale is instrumental for understanding details on molecular conformations and their dynamics.[7]

In the most common implementation, 2DIR is performed with sequences of three fs laser pulses, which are generated by splitting a parent pulse into replicas.[8] In this case, the frequency range of the excited and probed transitions is limited by the pulse bandwidth. It is of great value to be capable of measuring cross-peaks among modes of any given frequencies. In dual-frequency 2DIR, the frequencies of the laser pulses can be independently tuned to match the molecular vibrational transitions of interest, such that one can observe cross-peaks between vibrational modes with large frequency separation.[9,10] In cases where the modes of interest are not coupled directly, but are connected by pathways of intramolecular relaxation and transport, a relaxation-assisted dual-frequency 2DIR method is employed.[11,12] Recently, significant progress has been made toward developing experimental approaches to enable routine 2DIR measurements across a broad bandwidth, ultimately spanning the entire mid-infrared spectral range of molecular vibrational excitations.[13−15]

Received: July 24, 2019
Revised: September 8, 2019
Published: September 12, 2019

DOI: 10.1021/acs.jpcc.9b07045
J. Phys. Chem. C 2019, 123, 24731−24739

Traditional 2DIR cross-peak measurements are conducted with micrometer-thick samples of millimolar analyte concentrations. Similar measurements with thin films are difficult and limited to rather thick films exceeding 50 nm. The ability to enhance weak vibrational signals with localized fields of noble-metal plasmonic nanostructures opened an opportunity to study small amounts of surface molecules, down to a molecular monolayer.[16−20] For the efficient enhancement of molecular signals, plasmon resonances are tuned to match molecular transitions via control over the size and shape of the nanostructures.[21] However, the extension of surface-enhanced 2DIR (SE-2DIR) to dual-frequency experiments is not straightforward.[22] For dual-frequency measurements, the nanostructures should be capable of enhancing at the same time molecular transitions separated by many hundreds of wavenumbers. Moreover, the spatial distribution of the enhanced near-fields induced by the corresponding plasmonic excitations should coincide, such that different molecular transitions could be simultaneously enhanced in the same molecule.

Plasmonic excitations of the nanostructures desired for dual-frequency SE-2DIR should efficiently funnel the light of incident laser pulses into the near-field at the corresponding frequencies of the molecular transitions of interest. However, it is well-established that higher near-field enhancements are accompanied by narrower plasmonic excitations.[23] As a result, the structures with a single ultrabroad plasmonic band are not generally suitable for the task. High near-field enhancements are typically achieved with nanostructures involving nanometer-size gaps.[24−27] For example, very strong enhancement of the vibrational signals was recently obtained by Halas and co-workers with ultimately strong near-fields in the gap of antenna dimers, where advanced fabrication strategies were used to achieve gap sizes down to only a few nanometers and local field enhancement of over 3 orders of magnitude.[24] To obtain nanostructures supporting multiple plasmonic excitations, sophisticated shapes of the antennas comprising the dimer were developed by Maier and co-workers.[28]

In the present work, we demonstrate gold nanostructures that localize enhanced fields within the gap formed by the arms of a trimeric infrared antenna tailored for dual-frequency 2DIR experiments.[29] Because the cross-peak signals in 2DIR involve transitions at different frequencies, we exploit the symmetry properties of the trimer antennas to individually tune the frequencies of the two in-plane plasmonic excitations and to independently match their resonances with the corresponding vibrational transitions of interest. Localization of the enhanced field in the same spatial region within the gap for both in-plane plasmon excitations gives rise to a strong enhancement of the cross-peak signals observed in dual-frequency 2DIR experiments. In order to access the signal enhancement by the in-plane excitations of the trimer antenna, nonlinear spectroscopy is conducted with cross-polarized laser pulses.

Results of the polarization-selective dual-frequency 2DIR experiments indicate the superiority of our approach based on the plasmon mode engineering over the alternative structures supporting a single plasmonic excitation used in earlier studies.[22,30−32] Specifically, we focus on the benchmark molecule 4-azidobutyrate-*N*-hydroxysuccinimide ester (azNHS). We demonstrate that the cross-peak between the carbonyl stretching of the succinimide ester (transition frequency $\overline{\nu}_{CO}$ = 1745 cm^{-1}) and the azido stretching modes ($\overline{\nu}_{N3}$ = 2100 cm^{-1}), separated by ca. 370 cm^{-1}, is enhanced by an order of magnitude stronger in the trimer gap antenna having plasmonic excitations tuned in resonance with the molecular transitions (enhancement factor of ca. 10^4) as compared to the earlier experiments with half-wavelength bar antenna arrays.[22] Furthermore, we demonstrate similar signal enhancement for the cross-peak between the carbonyl stretching mode and the C−N−C asymmetric stretching mode of the succinimide group (transition frequency $\overline{\nu}_{CNC}$ = 1203 cm^{-1}) separated by ca. 550 cm^{-1}. Enhancement of cross-peaks with such greatly separated transition frequencies was not possible with the plasmonic arrays used in previous studies. Our results pave the way toward the application of the most advanced methods of nonlinear infrared spectroscopy to studies of thin molecular films on plasmonic nanostructures down to monolayers.

RESULTS AND DISCUSSION

Optical Properties of Symmetry-Broken Infrared Trimer Antennas. Noble-metal half-wavelength infrared antennas have been extensively used for linear surface-enhanced vibrational spectroscopy during the last decade.[21] The linear scaling of the plasmon resonance wavelength with the antenna length provides an intuitive guideline for tuning the plasmon excitation in resonance with the molecular transitions. In addition, arranging antennas into arrays with distances between antennas just below the critical period for grating diffraction conditions allows for enhancing the near-field next to the metal surface by the interantenna interaction.[33−35] Interestingly, our recent study of the linear and nonlinear signal enhancement in molecular films on half-wavelength infrared antenna arrays indicated that for films as thin as only a few nanometers, the origin of the enhanced signal cannot be localized to the region in the immediate proximity to the antenna surface, where the near-field is the strongest. We found that, generally, distant molecules also can significantly contribute to the enhanced signal via the radiative enhancement mechanism.[32] On the other hand, when the antennas involve narrow gaps, the measured signal originates in molecules located within the gap region.[29]

Upon excitation at the frequency of their plasmon resonance, individual half-wavelength infrared antennas have dipolar surface charge distribution, such that analogy between their optical properties and those of the subwavelength plasmonic nanoparticles can be readily drawn. Individual plasmonic nanoparticles are frequently described as point dipoles (plasmonic atoms), whereas interacting plasmonic nanoparticles are described as arrangements of such interacting dipoles (plasmonic molecules), whose collective excitations follow the symmetry of their geometrical arrangement.[36,37] When three nanoparticles are arranged at the vertices of an equilateral triangle having a D_{3h} symmetry, two degenerate bright bonding plasmon normal modes of the E′ symmetry emerge, having orthogonal orientation of their net dipole moments, such that they can be excited by light of appropriate polarization.[38] Similarly, when three half-wavelength antennas are arranged in a D_{3h} symmetric structure, two degenerate collective dipolar excitations associated with the bonding plasmon modes are observed in the infrared spectrum, as shown in Figure 1a for the gold nanostructures that we fabricated with electron beam lithography (EBL). Numerical simulations of the induced charge distributions on the antenna surface at the frequency of their plasmon resonance, shown in

DOI: 10.1021/acs.jpcc.9b07045
J. Phys. Chem. C 2019, 123, 24731−24739

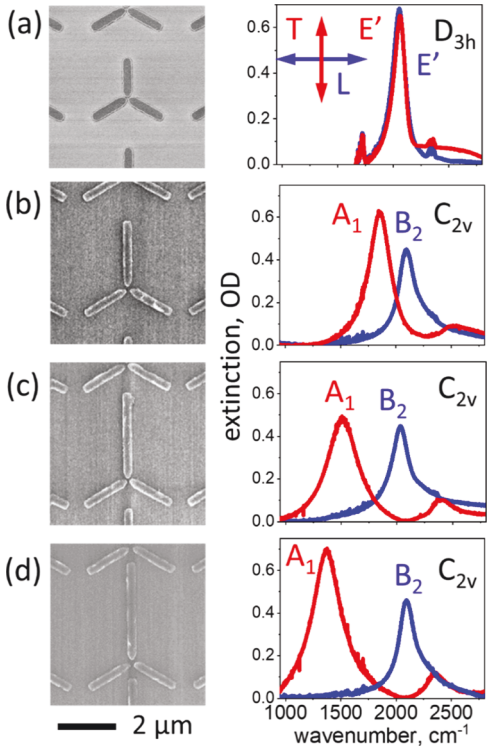

Figure 1. Symmetry-broken trimer infrared gold antenna. Left column: scanning electron micrographs of the antennas. The lengths of the two base arms of the trimer and of the central antenna are 1.25 and 1.25 μm in panel (a), 1.25 and 1.75 μm in panel (b), 1.3 and 2.3 μm in panel (c), and 1.25 and 2.6 μm in panel (d), respectively. The width of the antenna arms is 230 nm, height is 40 nm, and distances between the antennas' edges in the gap are 70 nm. The periodicity of the arrays is 3.1 μm along the direction of the central arm and 2.8 μm along the direction of the base arms. Right column: experimental polarization-selective extinction spectra. The orientation of the light polarization direction for each measurement with respect to the antennas is shown schematically in panel (a). The symmetry of the trimer antennas and their plasmon excitations are indicated.

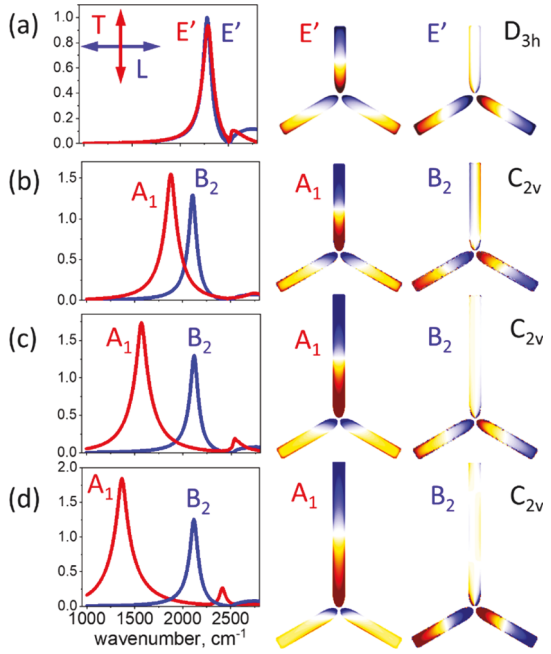

Figure 2. (a–d) Numerical simulations of the symmetry-broken trimer infrared gold antenna. Extinction spectra for different polarizations of the excitation light calculated for the antennas shown in Figure 1. Computed surface charge distributions induced at the frequency of plasmon resonance under the corresponding light polarization are shown. The symmetry of the trimer antennas and their plasmon excitations are indicated.

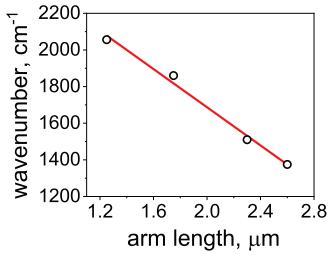

Figure 3. Tuning plasmon resonance via antenna geometry. Dependence of the resonance frequency of the A_1 bonding plasmon resonance on the length of the central arm of the trimer antenna. Circles—experimental data; red line—linear fit of the data: $\bar{\nu}$ = 2730 (±70) − 521 (±35)L, where $\bar{\nu}$—is the resonance frequency in cm^{-1} and L is the length of the central arm of the trimer in μm.

Figure 2a, reveal bright plasmon modes of the E′ symmetry with orthogonally oriented net dipole moments, as expected.

Breaking the symmetry of the D_{3h} trimer, for example, by changing the length of the central antenna arm, leads to splitting the degeneracy of the E′ excitations into those of the A_1 and B_2 symmetry of the C_{2v} group. The corresponding calculated charge distributions (Figure 2b–d) are fully consistent with the interpretation of the plasmonic excitations within the framework of the group theory.[36] In addition to the bonding plasmon modes, another weak antibonding resonance of the A_1 symmetry appears at the frequency of 2400 cm^{-1}, excited by the light polarized along the direction of the central arm of the antenna, as seen in Figure 1b–d. Although the resonance frequency of the bonding B_2 resonance does not change significantly (note that length of the two base arms of the trimer has not changed), the frequency of the bonding A_1 resonance shifts to the red as the central arm of the trimer becomes longer. Our results show that for the constant size of the gap, the spectral frequency shift of the A_1 resonance is linear with the length of the central arm of the trimer, as shown in Figure 3 for the series of trimers with gap sizes of 70 nm. Analogous behavior (results not shown) was observed also when the length of the arms in the base of the trimer was changed, consistent with observations made in similar systems.[27] Thus, by choosing the appropriate parameters of the antenna geometry, we are able to tune the plasmonic excitations of the trimer antennas to simultaneously match resonance conditions with different molecular vibrational modes, as desired for dual-frequency 2DIR experiments.

Surface-Enhanced Spectroscopy with Trimer Antennas. *Linear Spectroscopy.* The benchmark molecule for the dual-frequency 2DIR spectroscopy used in this study is azNHS (Figure 4a) dispersed in a polystyrene (PS) polymer film. azNHS has multiple bright vibrational transitions spanning the frequency range from ca. 1000 to 3000 cm^{-1}. In this study, we focused on cross-peaks involving the carbonyl stretching mode of the succinimide ester observed at the transition frequency of $\bar{\nu}_{CO}$ = 1745 cm^{-1}, C–N–C asymmetric stretching of the succinimide at $\bar{\nu}_{CNC}$ = 1203 cm^{-1}, and stretching of the azido moiety at $\bar{\nu}_{N3}$ = 2100 cm^{-1} (Figure 4b,c). Earlier relaxation-assisted dual-frequency 2DIR studies of azNHS revealed the

DOI: 10.1021/acs.jpcc.9b07045
J. Phys. Chem. C 2019, 123, 24731–24739

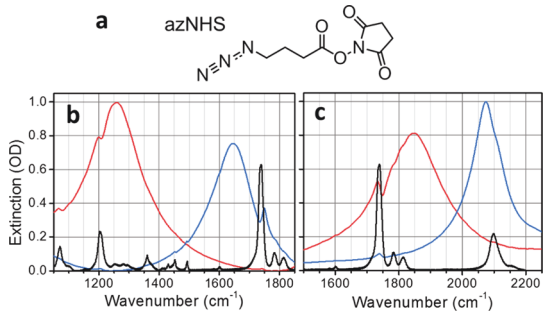

Figure 4. Linear spectroscopy of azNHS. (a) Molecular structure of azNHS. (b,c) Scaled (x5) absorption spectrum of 190 nm azNHS/PS film spin-coated onto a CaF_2 window is shown with black lines. Panels (b,c) also show polarized extinction spectra of the trimer arrays coated with a 10 nm film azNHS/PS with the polarization along the central bar (red lines) and perpendicular to it (blue lines), following the color code of Figures 1 and 2. The length of the trimers' arms are 1.75 and 2.6 μm (panel b) and 1.25 and 1.8 μm (panel c).

pathways and characteristic times of the excitation energy flow between these vibrational modes.[13] For example, it was found that it takes 7 ps for the excess vibrational energy on the carbonyl of the succinimide group ($\bar{\nu}_{CO}$ mode) to propagate through the molecule to the vicinity of the azide group ($\bar{\nu}_{N3}$ mode), whereas the relaxation within the succinimide between $\bar{\nu}_{CO}$ and $\bar{\nu}_{CNC}$ modes occurs within a few hundred femtoseconds.

Following the linear dependence of the plasmon resonance frequencies on the length of the antenna arms, we designed and fabricated trimer antenna arrays having resonances tailored to match specific pairs of the molecular vibrational transitions. The trimers designed to enhance transitions leading to the $\bar{\nu}_{CO}/\bar{\nu}_{CNC}$ cross-peak signals had arm lengths of 1.75 and 2.6 μm. These trimers are hereafter referred to as "Trimer array A". The trimers designed to enhance transitions of the $\bar{\nu}_{CO}/\bar{\nu}_{NN}$ cross-peak signals, arm lengths of 1.25 and 1.8 μm, are referred to as "Trimer array B". The corresponding linear spectra of these arrays coated by a 10 nm-thick azNHS/PS film are shown in Figure 4b,c. The thickness of the film was chosen to avoid possible contribution from the radiative interaction between the molecules and antennas.[32]

The effective field enhancements, evaluated for the linear extinction measurements (Figure 4b,c), were found to generally follow the plasmon near-field intensity at the corresponding transition frequency (see Figure 6 below), in full agreement with the observations reported in previous studies.[32] The optical density of the enhanced linear signals and the corresponding enhancement factors (EF_{FTIR}) are summarized in Table 1 for the polarization of the excitation light along the central arm of the trimer (denoted as a transverse polarization, ⟨T⟩) and perpendicular to it (denoted as a longitudinal polarization, ⟨L⟩). The reference signal for the $\bar{\nu}_{CO}$ and $\bar{\nu}_{NN}$ transitions was measured outside of the array region on the coated window with unpolarized light. The $\bar{\nu}_{CNC}$ transition in the reference sample of the same thickness was too weak to measure; thus, a thicker reference sample was used, and the ratio between the $\bar{\nu}_{CNC}$ and $\bar{\nu}_{CO}$ signals was used to determine the $\bar{\nu}_{CNC}$ intensity for the 10 nm reference sample. It was determined in our previous work that the concentration of the guest azNHS molecules decreases with the decrease in the PS film thickness.[22] Thus, for measurements referenced to thicker samples, both the concentration and thickness were accounted for when determining the raw enhancement. More details about the signal referencing are given in the Supporting Information.

Table 1. Enhancement of Linear Signal by Trimer Antennas

polarization	CO (mOD)	EF_{FTIR}	CNC (mOD)	EF_{FTIR}
	Trimer Array A			
⟨T⟩	8.3	6.9	88	195
⟨L⟩	138	114	10	22
reference	1.2	1	0.45[a]	1
polarization	CO (mOD)	EF_{FTIR}	NN (mOD)	EF_{FTIR}
	Trimer Array B			
⟨T⟩	133	160	7.0	29
⟨L⟩	26	32	28	116
reference	0.83	1	0.24	1

[a]Evaluated based on the ratio of CO/CNC peak amplitudes in 190 nm thick film.

As illustrated in Table 1, the signal enhancement is much stronger for light polarization accessing the plasmonic excitation in resonance with the vibrational transition. Enhancement of the linear signal of over a 100 was achieved for all the transitions of interest. Note, that because continuous polymer films are used in our experiments, the enhancement factors reported here correspond to the so-called raw-signal enhancement. The raw-signal enhancement was evaluated as the ratio of the measured signal amplitudes in films with and without plasmonic arrays obtained at the equivalent experimental conditions, similar to our earlier reports.[32] The raw-signal enhancement factors account for all the molecules in the sample without correction for the degree of their contribution to the total signal, which is affected by their location with respect to the region of the strongest near-field.

Dual-Frequency SE-2DIR: Trimer Array A. The magnitudes of linear signal enhancement in Table 1 provide a predictive measure for enhancements of the cross-peak signals in the 2DIR experiments.[22] Generally, enhancement of the 2DIR signals collected with the laser pulses of the same polarization followed the squared values of the enhancements measured in the linear experiments for the diagonal peaks and the products of the corresponding enhancement values obtained for the relevant molecular transitions for the cross-peaks. Consider the Trimer array A, having plasmonic resonances at ca. 1650 and 1250 cm^{-1}, excited by ⟨L⟩ and ⟨T⟩ light polarization, respectively (see Figure 4b for linear spectrum). When a single polarization is used in 2DIR experiments, pulse sequences ⟨LLLL⟩ or ⟨TTTT⟩, strong enhancement of the molecular signals is only available at one of the transition frequencies involved. Indeed, for the 2DIR spectrum shown in Figure 5a, collected with the ⟨LLLL⟩ pulse polarizations, the raw 2DIR signal enhancement, EF_{2DIR}, of the diagonal CO peak was ca. 3×10^3, as all pulses excited the plasmon mode having resonance close to the $\bar{\nu}_{CO}$ transition. On the other hand, the raw EF_{2DIR} for the CO diagonal peak was an order of magnitude lower for the measurements with ⟨LLTT⟩ polarizations (Figure 5c), where the ⟨T⟩-polarized pulses excite plasmonic mode whose resonance is far away from the $\bar{\nu}_{CO}$ transition. Similarly, when the CO/CNC cross-peak was measured with the ⟨LLLL⟩ polarization (Figure 5b), the $\bar{\nu}_{CNC}$ transition is not enhanced by the resonant interaction with the plasmon and the raw EF_{2DIR} is relatively low. On the other hand, when ⟨LLTT⟩ polarizations of the pulses are used (Figure 5d), both plasmonic resonances are engaged in the

DOI: 10.1021/acs.jpcc.9b07045
J. Phys. Chem. C 2019, 123, 24731−24739

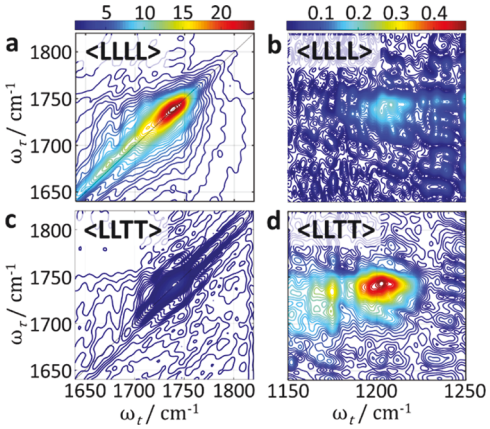

Figure 5. Dual-frequency SE-2DIR spectroscopy of azNHS on Trimer array A. Diagonal CO peak measured with (a) ⟨LLLL⟩ and (c) ⟨LLTT⟩ polarizations. CO/CNC cross-peak measured with (b) ⟨LLLL⟩ and (d) ⟨LLTT⟩ polarizations. The 2DIR spectra were measured at the waiting time of 0.2 ps.

signal enhancement and the signal of the CO/CNC cross-peak was enhanced by a factor of 5.6×10^3. The measured EF_{2DIR} values are summarized in Table 2. The off-gold reference measurements were performed at a 10-fold higher laser power to facilitate measuring a stronger signal (Figure S1), and these laser powers were used when calculating the raw enhancement. See the Supporting Information for more details on signal referencing.

It is important to note here a difference between the experiments conducted with cross-polarized laser pulses on the samples with and without plasmonic antenna. In bulk isotropic samples, averaging over all possible molecular orientations reduces diagonal peak signals collected with cross-polarized laser pulses by a factor of 3, as compared to that collected with all-parallel pulse polarizations.[39] The amplitudes of the cross-peaks are also affected by the polarization conditions, depending on the relative angles of the involved transition dipoles. On the contrary, our recent single-color SE-2DIR experiments with symmetric trimer antennas (similar to that in Figure 1a) have shown that despite different polarizations of the laser pulses were used, the enhanced molecular signals were excited by the electric field of the same polarization.[29] This observation indicates that in the case of trimer antennas, the molecules that are located close to the metal surface interact with the local electric field, whose direction is governed by the surface boundary conditions.[40,41] Therefore, the 2DIR spectra of the reference sample, the coated window outside of the array region, were collected with all-parallel pulse polarizations.

Another important consideration for evaluation of the actual EF_{2DIR} values is the effective volume occupied by molecules contributing to the SE signal, V_{eff}. It has been previously shown that for the films thinner than 10 nm,[22] for arrays with periodicity significantly shorter than the wavelength of the molecular transitions,[33] and especially for plasmonic antenna geometries involving gaps,[29] the magnitude of the enhanced signal is correlated with the strength of the near-field around plasmonic nanostructures. Thus, in order to estimate the amount of molecules contributing to the enhanced signal, we calculated the near-fields around the Trimer A. The near-field spectra calculated at the point located within the gap for the excitation with the ⟨L⟩ and ⟨T⟩ light polarizations are shown in Figure 6a. The spatial distributions of the near-fields at the molecular transition frequencies and for the appropriate polarizations of the excitation light are shown in Figure 6b,c. The simulation results predict up to 2 orders of magnitude enhancement of the near-field in the gap region. Because the amplitude of the third-order cross-peak signal scales with the product of the squares of the near-field amplitudes, we also plotted the corresponding products of these near-fields in Figure 6d. As it is seen from the figure, a very strong signal enhancement factor of above 10^6 is calculated for molecules residing within the narrow gap between the antenna arms, which is ca. 100 times higher than the enhancements calculated previously for the array of half-wavelength antennas.[22] In these simulations, we used a 70 nm gap size, similar to that in our experimentally fabricated antennas. Narrowing the gap down to 40 nm leads to increase of the signal enhancement factor above 10^8.

In order to evaluate the effective sampled volume, V_{eff}, we analyzed the results of the numerical simulations assuming that

Table 2. Enhancement of 2DIR Signals by Trimer Antennas

	CO/CO			CO/CNC		
polarization	EF_{2DIR}, raw	effective volume, $\times 10^{-3}$ μm^3	EF_{2DIR}, corrected	EF_{2DIR}, raw	effective volume, $\times 10^{-3}$ μm^3	EF_{2DIR}, corrected
			Trimer Array A			
⟨TTTT⟩	470	11.0	170	1400	12.0	75
⟨LLLL⟩	3200	5.4	2370	2340	4.9	299
⟨LLTT⟩	350	4.0	350	5600	0.64	5600
⟨TTLL⟩	320	4.0	320		0.64	
reference	1	78	1	1[a]	78	1
	CO/CO			CO/NN		
polarization	EF_{2DIR}, raw	effective volume, $\times 10^{-3}$ μm^3	EF_{2DIR}, corrected	EF_{2DIR}, raw	effective volume, $\times 10^{-3}$ μm^3	EF_{2DIR}, corrected
			Trimer Array B			
⟨TTTT⟩	18 000	6.5	1800	7400	6.5	740
⟨LLLL⟩	4700	4.0	790	4100	4.0	650
⟨LLTT⟩	2800	0.67	2800	320	0.63	320
⟨TTLL⟩	3200	0.67	3200	7000	0.63	7000
reference	1	78	1	1[b]	78	1

[a]Evaluated with 190 nm-thick film; diagonal-to-cross peak amplitudes ratio is 84. [b]Evaluated with 190 nm-thick film; sample diagonal-to-cross peak amplitude ratio is 66.

DOI: 10.1021/acs.jpcc.9b07045
J. Phys. Chem. C 2019, 123, 24731−24739

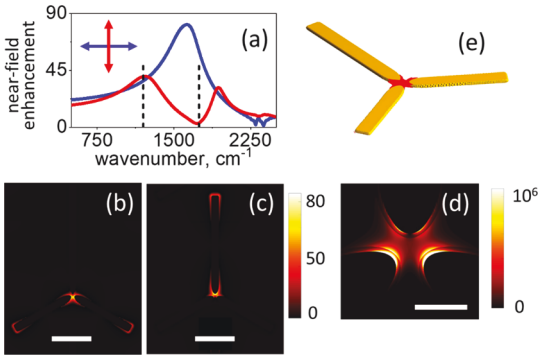

Figure 6. Near-fields around antenna of Trimer array A. (a) Spectra of the near-field excited by ⟨T⟩ (red line) and ⟨L⟩ (blue) light polarization. The spectra are evaluated at the gap, at the location, where the cross-peak signal is maximized, see panel (d). Transition frequencies of the CO ($\bar{\nu}_{CO}$ = 1745 cm^{-1}) and CNC ($\bar{\nu}_{CNC}$ = 1200 cm^{-1}) modes are indicated with dashed lines. (b) Distribution of the near-field enhancement around the antenna for excitation at 1745 cm^{-1} with ⟨L⟩-polarized light (blue spectrum in panel a). Scale bar is 1 μm. (c) Same as in panel (b), but for excitation at 1200 cm^{-1} with ⟨T⟩-polarized light (red spectrum in panel (a). (d) Product of the square values of the fields in panels (b,c) representing the enhancement of the CO/CNC cross-peak signal in the polarization-selective dual-frequency 2DIR experiment. Scale bar is 200 nm. The simulation accounts also for the dielectric screening of the 10 nm thick PS film coating the antenna, n = 1.53. (e) Trimer antenna showing location of molecules (in red) contributing to 90% of the CO/CNC cross-peak signal.

the trimer antennas are homogeneously covered by a uniform 10 nm thick molecular film. This assumption is supported by our earlier imaging of the antenna cross-section.[31] In the simulation, the space of the array's unit cell was discretized into N volume elements. The signal contribution of the k-th element ΔV_k containing the film with sampled molecules to the total signal S_{tot} was assumed to be proportional to the relevant product of the enhanced fields' amplitudes, $S_k = |\vec{E}_k^{\langle i\rangle}|^2|\vec{E}_k^{\langle j\rangle}|^2\Delta V_k$, such that $S_{tot} = \sum_k^N S_k$. Here, i, j = T, L, according to the experimental conditions (see Figure 6d for illustration of the product $|\vec{E}^{\langle T\rangle}|^2|\vec{E}^{\langle L\rangle}|^2$). V_{eff} was calculated by summation of ΔV_k values corresponding to the highest values of S_k. The simulations revealed that V_{eff}, accounting for the 90% of the total third-order signal per unit cell of the antenna array, differs significantly for the cases where all-parallel and cross-polarized excitation pulses are used. For example, V_{eff} evaluated for the CO/CNC cross-peak for the ⟨LLTT⟩ excitation pulse polarizations corresponds to the area of 250 × 250 nm^2 of the 10 nm thick film located within the gap region of the trimer, as illustrated in Figure 6. In our experimental samples, this region includes only ca. 1.5 × 10^5 azNHS molecules. On the other hand, for the excitation with ⟨LLLL⟩ pulse polarizations, we obtained that V_{eff} is almost 10 times larger, corresponding to the region of 700 × 700 nm^2, which is located also outside the gap, as seen in Figure 6b,c. Following this observation, we have corrected the raw EF_{2DIR} values obtained for measurements with all-parallel polarized pulses in Table 2, by scaling them by the ratio of the V_{eff} values corresponding to the excitations by all-parallel and cross-polarized pulses. Such scaling normalizes the enhancement factors to the same number of molecules contributing to the enhanced signal and allows for their comparison. The corrected EF_{2DIR} values are summarized in Table 2, together with the associated values of V_{eff}.

Dual-Frequency SE-2DIR: Trimer Array B. Similar results were obtained in the case of the Trimer array B, where plasmonic resonances were tuned to enhance the CO/NN cross-peak with the corresponding excitations at 1850 and 2100 cm^{-1}, respectively (see Figure 4b for linear spectrum). The corresponding 2DIR spectra for the CO diagonal and CO/NN cross-peaks collected with the ⟨LLLL⟩ and ⟨TTLL⟩ pulse polarizations are shown in Figure 7. The data were

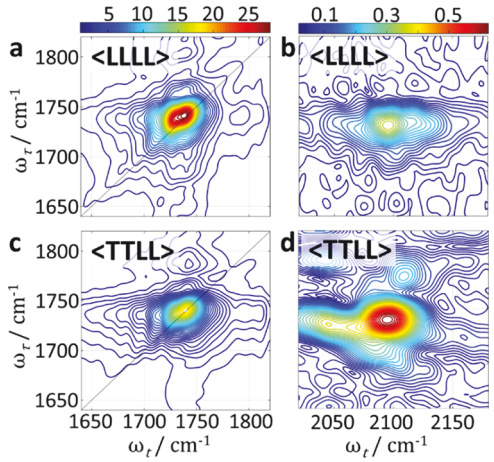

Figure 7. Dual-frequency SE-2DIR spectroscopy of azNHS on Trimer array B. (a) Diagonal CO peak measured with the ⟨LLLL⟩ polarizations of the laser pulses; (c) same as in (a) but with the ⟨TTLL⟩ polarizations. (b) CO/NN cross-peak measured with the ⟨LLLL⟩ pulse polarizations; (d) same as in (b) but with ⟨TTLL⟩ polarizations. Cross-peak spectra were measured at the waiting time of 7 ps. See Figure 4b for corresponding linear spectra.

collected for the waiting time of 7 ps, where the amplitude of the relaxation-assisted CO/NN cross-peak signal is maximal.[11−13] Results of the signal enhancement analysis are summarized in Table 2 together with the corresponding values of V_{eff}. The EF_{2DIR} value for the CO/NN cross-peak signal obtained with the trimer antennas was 7 × 10^3, which can be readily compared with our earlier results, where the EF_{2DIR} value of 6 × 10^2 was obtained with a single broadband plasmonic resonance.[22] The order-of-magnitude increase in the signal is a direct manifestation of the role plasmon resonances of the trimer antenna play in the enhancement of the cross-peak signals. Note that such comparison is not possible for the CO/CNC cross-peak enhanced by the Trimer array A discussed above because frequency separation of ca. 550 cm^{-1} between the $\bar{\nu}_{CO}$ and $\bar{\nu}_{CNC}$ transitions is too large for a substantial enhancement of this cross-peak by a single plasmon excitation with a typical bandwidth of ca. 250 cm^{-1}.

Notice that the raw cross-peak enhancement values of 6 to 7 × 10^3 fold were obtained in reference to a sample film of the same thickness on CaF_2. If these EF_{2DIR} values are corrected for the effective sample volume contributing to the signal in both cases, much larger enhancement values of (5600 × 78/0.64=) 7 × 10^5 and 9 × 10^5 are obtained for the CO/CNC and CO/NN cross-peaks on trimer antennas, respectively. These values suggest that the mean near-field enhancement, affecting the 10 nm-thick sample, is ca. 30-fold.

CONCLUSIONS

To summarize, we have demonstrated how symmetry properties of trimer infrared antenna can be exploited to

DOI: 10.1021/acs.jpcc.9b07045
J. Phys. Chem. C 2019, 123, 24731−24739

design their plasmon resonances in a way that allows significant enhancement of the cross-peak signals in dual-frequency surface-enhanced 2DIR measurements of thin molecular films. Specifically, two in-plane plasmonic modes of the trimer antenna with orthogonal dipole moments can be independently tuned in resonance with the molecular transitions of interest. Illumination of the trimer structure by the cross-polarized laser pulses allows selectively engaging these plasmon excitations to enhance the relevant molecular transitions. We validate our approach by demonstrating a nearly 10^4-fold raw-signal enhancement of the cross-peak signal for molecular transitions separated in frequency by ca. 550 cm^{-1}, which could not be achieved earlier with plasmonic structures involving a single broadband excitation. Enhancement of the third-order signals from molecules residing within the gap of the antenna is possible because of the up to 100-fold enhancement of the near-field inside the gap. Trimers used in the present study have gaps of 70 nm; further reducing the gap size will dramatically increase the strength of the enhanced field. It is anticipated that nanometer-scale confinement affects molecular structure and dynamics in thin films. While our present report focuses on the methodology needed to achieve the signal enhancement, we will pursue the studies of molecular structure and dynamics in thin films in the following work. Note, however, that the field enhancement factors of 50−100 correspond to a highly nonlinear regime of the molecule−field interaction. We are actively exploring how these strong fields affect nonlinear molecular spectroscopy.

EXPERIMENTAL METHODS

Fabrication of Trimer Arrays. Gold infrared trimer antenna arrays were fabricated by EBL on thoroughly-cleaned CaF_2 windows. The windows were coated by hexamethyldisilazane using vapor deposition (automatic Coater Suss MicroTec Delta 80 RC). A negative slope pattern was created by double-layer PMMA resists (495-A2 and 950 A3, MicroChem) in two steps, which included baking after each coating. A 30 nm layer of chromium was deposited with an e-beam evaporator (Temescal FC-1800, base pressure $<5 \times 10^{-7}$ Torr) to have good conductivity and optical reflectance for the EBL. The antenna pattern was made on a RAITH, EBPG 5200 instrument. Each array had a total area of 4 mm × 4 mm. The exposed pattern was developed first in chromium etchant solution (Micro Chemicals) and then in methyl isobutyl ketone−isopropanol 1:3 mixture (MicroChem). After development, a 5 nm chromium adhesion layer and 40 nm of gold were deposited with an e-beam evaporator (Temescal FC-1800). Finally, the lift-off was done with acetone, and the antenna array sample was spin-coated with the azNHS/PS film.

Sample Preparation. azNHS was purchased from Synthonix, Inc. Thin-film samples of azNHS dispersed in PS of molecular weight of 35 kDa were prepared by spin coating a toluene solution of azNHS/PS. The azNHS/PS film thickness and concentration (0.4 M) on the nanoarray were determined by previous studies.[22]

Infrared Spectroscopy. Linear FTIR measurements were performed in transmission mode with a Vertex 80 spectrometer (Bruker). A gold, wire-grid polarizer was placed in the sample cell compartment to measure the spectral contributions stemming from light polarization parallel and perpendicular to the trimer central axis separately without moving the sample. Additionally, an aperture of ca. 1 mm in diameter was placed in front of the sample to limit the measured area to the location of the array.

Two-Dimensional Infrared Spectroscopy. A fully automated dual-frequency three-pulse 2DIR spectrometer with heterodyned detection is described in detail elsewhere.[13] The spectrometer is powered by a Ti:sapphire laser (Libra, Coherent) which produces 1.5 W power at a 1 kHz repetition rate and 80 fs pulse duration. Mid-IR pulses of ca. 150 fs duration were generated with a dual optical parametric amplifier and difference frequency generation units. The energy of the pump and probe pulses was reduced to 80 and 10 nJ, respectively, to prevent light-induced degradation of the nanoantenna arrays. Half-wave plates and wire-grid polarizers were placed on the pump beams paths to allow for polarization control in the cross-polarized measurements. Further experimental details are provided in the Supporting Information.

Numerical Simulations. Numerical simulations of the optical properties of infrared trimer antenna were done with the FDTD method using Lumerical software. The geometry of the gold antenna in each simulation was obtained from the corresponding scanning electron microscopy images; the width of the antenna bars was 250 nm, the height was 40 nm, and the length was varied as in the experiments. We used the gold dielectric function from Johnson and Christy.[42] The effective refractive index of the surrounding medium of $n = 1.2$ was used to mimic the effect of CaF_2 substrate. The excitation was by plane wave at the normal incidence with absorbing boundary conditions along the light propagation direction. The possible interaction between the neighboring trimers in the array was described by using the corresponding periodic boundary conditions. In order to calculate the detailed near-field distribution within the antenna gap, fine meshing of this region was used with the element size down to 0.5 nm in the areas close to the metal surface. In order to reduce the computational efforts, we used symmetric or anti-symmetric boundary conditions for the electric and magnetic fields with respect to the σ_v reflection plane of the trimer. For the PS film, $n = 1.53$ was used.

ASSOCIATED CONTENT

Supporting Information

The Supporting Information is available free of charge on the ACS Publications website at DOI: 10.1021/acs.jpcc.9b07045.

Details on the experimental methods, referencing for the enhancement calculations, and a 2DIR reference spectrum (PDF)

AUTHOR INFORMATION

Corresponding Authors

*E-mail: irubtsov@tulane.edu, (I.V.R.).
*E-mail: chunt@technion.ac.il (L.C.).

ORCID

Igor V. Rubtsov: 0000-0002-3010-6207
Lev Chuntonov: 0000-0002-2316-4708

Author Contributions

⊥R.T.M. and B.C. contributed equally.

Notes

The authors declare no competing financial interest.

DOI: 10.1021/acs.jpcc.9b07045
J. Phys. Chem. C 2019, 123, 24731−24739

■ ACKNOWLEDGMENTS

This research is supported by Grant 2016167 from the United States−Israel Binational Science Foundation (BSF). Plasmonic arrays were prepared at the Micro- and Nano-Fabrication Unit, Technion, with support from the Russell Berrie Nanotechnology Institute. The support by the United States National Science Foundation (CHE-1900568 to I.R.) and by Israel Science Foundation (1118/15 to L.C.) is gratefully acknowledged.

■ REFERENCES

(1) Wilson, E. B.; Decius, J. C.; Cross, P. C. *Molecular Vibrations*; Dover: New York, 1955.
(2) Hoşafçı, G.; Klein, O.; Oremek, G.; Mäntele, W. Clinical Chemistry without Reagents? An Infrared Spectroscopic Technique for Determination of Clinically Relevant Constituents of Body Fluids. *Anal. Bioanal. Chem.* **2007**, *387*, 1815.
(3) Hamm, P. For structural biology, try infrared instead. *Structure* **2009**, *17*, 149−150.
(4) Hamm, P.; Zanni, M. T. *Concepts and Methods of 2D Infrared Spectroscopy*; Cambridge University Press: Cambridge, 2011.
(5) Hamm, P.; Lim, M.; Hochstrasser, R. M. Structure of the Amide I Band of Peptides Measured by Femtosecond Nonlinear-Infrared Spectroscopy. *J. Phys. Chem. B* **1998**, *102*, 6123−6138.
(6) Golonzka, O.; Khalil, M.; Demirdöven, N.; Tokmakoff, A. Coupling and Orientation between Anharmonic Vibrations Characterized with Two-Dimensional Infrared Vibrational Echo Spectroscopy. *J. Chem. Phys.* **2001**, *115*, 10814−10828.
(7) Ganim, Z.; Chung, H. S.; Smith, A. W.; DeFlores, L. P.; Jones, K. C.; Tokmakoff, A. Amide I Two-Dimensional Infrared Spectroscopy of Proteins. *Acc. Chem. Res.* **2008**, *41*, 432−441.
(8) Asplund, M. C.; Zanni, M. T.; Hochstrasser, R. M. Two-Dimensional Infrared Spectroscopy of Peptides by Phase-Controlled Femtosecond Vibrational Photon Echoes. *Proc. Natl. Acad. Sci. U.S.A.* **2000**, *97*, 8219−8224.
(9) Rubtsov, I. V.; Wang, J.; Hochstrasser, R. M. Dual-Frequency 2D-IR Spectroscopy Heterodyned Photon Echo of the Peptide Bond. *Proc. Natl. Acad. Sci. U.S.A.* **2003**, *100*, 5601−5606.
(10) Rubtsov, I. V.; Kumar, K.; Hochstrasser, R. M. Dual-Frequency 2D IR Photon Echo of a Hydrogen Bond. *Chem. Phys. Lett.* **2005**, *402*, 439−443.
(11) Rubtsov, I. V. Relaxation-Assisted Two-Dimensional Infrared (RA 2DIR) Method: Accessing Distances over 10 Å and Measuring Bond Connectivity Patterns. *Acc. Chem. Res.* **2009**, *42*, 1385−1394.
(12) Rubtsov, I. V. In *Ultrafast Infrared Vibrational Spectroscopy*; Fayer, M. D., Ed.; CRC Press, 2013.
(13) Leger, J. D.; Nyby, C. M.; Varner, C.; Tang, J.; Rubtsova, N. I.; Yue, Y.; Kireev, V. V.; Burtsev, V. D.; Qasim, L. N.; Rubtsov, G. I.; Rubtsov, I. V. Fully Automated Dual-Frequency Three-Pulse-Echo 2DIR Spectrometer Accessing Spectral Range from 800 to 4000 Wavenumbers. *Rev. Sci. Instrum.* **2014**, *85*, 083109.
(14) Petersen, P. B.; Tokmakoff, A. Source for Ultrafast Continuum Infrared and Terahertz Radiation. *Opt. Lett.* **2010**, *35*, 1962−1964.
(15) Stingel, A. M.; Vanselous, H.; Petersen, P. B. Covering the Vibrational Spectrum with Microjoule Mid-Infrared Supercontinuum Pulses in Nonlinear Optical Applications. *J. Opt. Soc. Am. B* **2017**, *34*, 1163−1169.
(16) Kraack, J. P.; Hamm, P. Surface-Sensitive and Surface-Specific Ultrafast Two-Dimensional Vibrational Spectroscopy. *Chem. Rev.* **2016**, *117*, 10623−10664.
(17) Selig, O.; Siffels, R.; Rezus, Y. L. A. Ultrasensitive Ultrafast Vibrational Spectroscopy Employing the near Field of Gold Nanoantennas. *Phys. Rev. Lett.* **2015**, *114*, 233004.
(18) Kusa, F.; Morichika, I.; Takegami, A.; Ashihara, S. Enhanced Ultrafast Infrared Spectroscopy Using Coupled Nanoantenna Arrays. *Opt. Express* **2017**, *25*, 12896−12907.
(19) Morichika, I.; Kusa, F.; Takegami, A.; Sakurai, A.; Ashihara, S. Antenna-Enhanced Nonlinear Infrared Spectroscopy in Reflection Geometry. *J. Phys. Chem. C* **2017**, *121*, 11643−11649.
(20) Li, N.; Yin, H.; Zhuo, X.; Yang, B.; Zhu, X.-M.; Wang, J. Infrared-Responsive Colloidal Silver Nanorods for Surface-Enhanced Infrared Absorption. *Adv. Opt. Mater.* **2018**, *6*, 1800436.
(21) Neubrech, F.; Huck, C.; Weber, K.; Pucci, A.; Giessen, H. Surface-Enhanced Infrared Spectroscopy Using Resonant Nanoantennas. *Chem. Rev.* **2017**, *117*, 5110−5145.
(22) Mackin, R. T.; Cohn, B.; Gandman, A.; Leger, J. D.; Chuntonov, L.; Rubtsov, I. V. Surface-Enhanced Dual-Frequency Two-Dimensional Vibrational Spectroscopy of Thin Layers at an Interface. *J. Phys. Chem. C* **2018**, *122*, 11015−11023.
(23) Zhang, Y.; Wen, F.; Zhen, Y.-R.; Nordlander, P.; Halas, N. J. Coherent Fano Resonances in a Plasmonic Nanocluster Enhance Optical Four-Wave Mixing. *Proc. Nat. Acad. Sci.* **2013**, *110*, 9215−9219.
(24) Dong, L.; Yang, X.; Zhang, C.; Cerjan, B.; Zhou, L.; Tseng, M. L.; Zhang, Y.; Alabastri, A.; Nordlander, P.; Halas, N. J. Nanogapped Au Antennas for Ultrasensitive Surface-Enhanced Infrared Absorption Spectroscopy. *Nano Lett.* **2017**, *17*, 5768−5774.
(25) Neubrech, F.; Weber, D.; Katzmann, J.; Huck, C.; Toma, A.; Di Fabrizio, E.; Pucci, A.; Härtling, T. Infrared Optical Properties of Nanoantenna Dimers with Photochemically Narrowed Gaps in the 5 Nm Regime. *ACS Nano* **2012**, *6*, 7326−7332.
(26) Brown, L. V.; Yang, X.; Zhao, K.; Zheng, B. Y.; Nordlander, P.; Halas, N. J. Fan-Shaped Gold Nanoantennas above Reflective Substrates for Surface-Enhanced Infrared Absorption (SEIRA). *Nano Lett.* **2015**, *15*, 1272−1280.
(27) Brown, L. V.; Zhao, K.; King, N.; Sobhani, H.; Nordlander, P.; Halas, N. J. Surface-Enhanced Infrared Absorption Using Individual Cross Antennas Tailored to Chemical Moieties. *J. Am. Chem. Soc.* **2013**, *135*, 3688−3695.
(28) Aouani, H.; Šípová, H.; Rahmani, M.; Navarro-Cia, M.; Hegnerová, K.; Homola, J.; Hong, M.; Maier, S. A. Ultrasensitive Broadband Probing of Molecular Vibrational Modes with Multifrequency Optical Antennas. *ACS Nano* **2012**, *7*, 669−675.
(29) Cohn, B.; Engelman, B.; Goldner, A.; Chuntonov, L. Two-Dimensional Infrared Spectroscopy with Local Plasmonic Fields of a Trimer Gap-Antenna Array. *J. Phys. Chem. Lett.* **2018**, *9*, 4596−4601.
(30) Cohn, B.; Prasad, A. K.; Chuntonov, L. Communication: Probing the Interaction of Infrared Antenna Arrays and Molecular Films with Ultrafast Quantum Dynamics. *J. Chem. Phys.* **2018**, *148*, 131101.
(31) Gandman, A.; Mackin, R.; Cohn, B.; Rubtsov, I. V.; Chuntonov, L. Two-Dimensional Fano Lineshapes in Ultrafast Vibrational Spectroscopy of Thin Molecular Layers on Plasmonic Arrays. *J. Phys. Chem. Lett.* **2017**, *8*, 3341−3346.
(32) Gandman, A.; Mackin, R. T.; Cohn, B.; Rubtsov, I. V.; Chuntonov, L. Radiative Enhancement of Linear and Third-Order Vibrational Excitations by an Array of Infrared Plasmonic Antennas. *ACS Nano* **2018**, *12*, 4521−4528.
(33) Adato, R.; Yanik, A. A.; Amsden, J. J.; Kaplan, D. L.; Omenetto, F. G.; Hong, M. K.; Erramilli, S.; Altug, H. Ultra-Sensitive Vibrational Spectroscopy of Protein Monolayers with Plasmonic Nanoantenna Arrays. *Proc. Nat. Acad. Sci.* **2009**, *106*, 19227−19232.
(34) Bagheri, S.; Weber, K.; Gissibl, T.; Weiss, T.; Neubrech, F.; Giessen, H. Fabrication of Square-Centimeter Plasmonic Nanoantenna Arrays by Femtosecond Direct Laser Writing Lithography: Effects of Collective Excitations on Seira Enhancement. *ACS Photonics* **2015**, *2*, 779−786.
(35) Simpkins, B. S.; Long, J. P.; Glembocki, O. J.; Guo, J.; Caldwell, J. D.; Owrutsky, J. C. Pitch-Dependent Resonances and near-Field Coupling in Infrared Nanoantenna Arrays. *Opt. Express* **2012**, *20*, 27725−27739.
(36) Haran, G.; Chuntonov, L. Artificial Plasmonic Molecules and Their Interaction with Real Molecules. *Chem. Rev.* **2018**, *118*, 5539−5580.

DOI: 10.1021/acs.jpcc.9b07045
J. Phys. Chem. C 2019, 123, 24731−24739

(37) Brandl, D. W.; Mirin, N. A.; Nordlander, P. Plasmon Modes of Nanosphere Trimers and Quadrumers. *J. Phys. Chem. B* **2006**, *110*, 12302−12310.
(38) Chuntonov, L.; Haran, G. Trimeric Plasmonic Molecules: The Role of Symmetry. *Nano Lett.* **2011**, *11*, 2440−2445.
(39) Hochstrasser, R. M. Two-Dimensional IR-Spectroscopy: Polarization Anisotropy Effects. *Chem. Phys.* **2001**, *266*, 273−284.
(40) Moskovits, M.; Suh, J. S. Surface Selection Rules for Surface-Enhanced Raman Spectroscopy: Calculations and Application to the Surface-Enhanced Raman Spectrum of Phthalazine on Silver. *J. Phys. Chem.* **1984**, *88*, 5526−5530.
(41) Greenler, R. G.; Snider, D. R.; Witt, D.; Sorbello, R. S. The Metal-Surface Selection Rule for Infrared Spectra of Molecules Adsorbed on Small Metal Particles. *Surf. Sci.* **1982**, *118*, 415−428.
(42) Johnson, P. B.; Christy, R. W. Optical Constants of the Noble Metals. *Phys. Rev. B: Solid State* **1972**, *6*, 4370−4379.

DOI: 10.1021/acs.jpcc.9b07045
J. Phys. Chem. C 2019, 123, 24731−24739